BMC Genomics

RESEARCH Open Access

Cell-specific AHR-driven differential gene expression in the mouse liver cell following acute TCDD exposure

Giovan N. Cholico[1,2], Rance Nault[2,3] and Tim Zacharewski[1,2*]

Abstract

2,3,7,8-Tetrachlorodibenzo-*p*-dioxin (TCDD) is a persistent environmental contaminant that disrupts hepatic function leading to steatotic liver disease (SLD)-like pathologies, such as steatosis, steatohepatitis, and fibrosis. These effects are mediated by the aryl hydrocarbon receptor following changes in gene expression. Although diverse cell types are involved, initial cell-specific changes in gene expression have not been reported. In this study, differential gene expression in hepatic cell types was examined in male C57BL/6 mice gavaged with 30 µg/kg of TCDD using single-nuclei RNA-sequencing. Ten liver cell types were identified with the proportions of most cell types remaining unchanged, except for neutrophils which increased at 72 h. Gene expression suggests TCDD induced genes related to oxidative stress in hepatocytes as early as 2 h. Lipid homeostasis was disrupted in hepatocytes, macrophages, B cells, and T cells, characterized by the induction of genes associated with lipid transport, steroid hormone biosynthesis, and the suppression of β-oxidation, while linoleic acid metabolism was altered in hepatic stellate cells (HSCs), B cells, portal fibroblasts, and plasmacytoid dendritic cells. Pro-fibrogenic processes were also enriched, including the induction retinol metabolism genes in HSCs and the early induction of anti-fibrolysis genes in hepatocytes, endothelial cells, HSCs, and macrophages. Hepatocytes also had gene expression changes consistent with hepatocellular carcinoma. Collectively, these findings underscore the effects of TCDD in initiating SLD-like phenotypes and identified cell-specific gene expression changes related to oxidative stress, steatosis, fibrosis, cell proliferation and the development of HCC.

Keywords 2,3,7,8-tetrachlorodibenzo-*p*-dioxin (TCDD), Aryl hydrocarbon receptor (AHR), Liver, Toxicogenomics, Single-nuclei RNA-sequencing (snRNAseq)

*Correspondence:
Tim Zacharewski
tzachare@msu.edu
[1]Biochemistry and Molecular Biology, Michigan State University, East Lansing, Michigan, USA
[2]Institute for Integrative Toxicology, Michigan State University, East Lansing, Michigan, USA
[3]Pharmacology and Toxicology, Michigan State University, East Lansing, Michigan, USA

Background

The aryl hydrocarbon receptor (AHR) is a ligand-activated transcription factor that plays a pivotal role in mediating cellular responses. In addition to serving as a sensor, in response to environmental contaminants such as polychlorinated dibenzo-*p*-dioxins (PCDDs), dibenzofurans (PCDFs), and biphenyls (PCBs), the AHR can also be activated by a growing list of structurally diverse endogenous intermediates, microbial metabolites, and natural products [1]. Upon activation, the AHR facilitates differential gene expression through a process where the cytosolic AHR releases associated chaperone proteins and translocates into the nucleus. There, it forms a complex with the AHR nuclear translocator (ARNT) [1]. This AHR/ARNT heterodimer complex then binds to specific DNA sequences called dioxin response elements (DREs) within the locus of target genes, triggering gene transcription. The most potent and prototypical AHR ligand is 2,3,7,8-tetrachlorodibenzo-*p*-dioxin (TCDD), a persistent environmental contaminant that elicits chloracne [2], immune system suppression [3], impaired fertility [4], and liver disease pathologies including hepatocellular carcinoma (HCC) [1, 5]. Although the mechanism of TCDD toxicity is unresolved, knock-out studies demonstrate the effects are due to differential gene expression mediated by the AHR [6].

In the mouse liver, TCDD induces pathologies observed in steatotic liver disease (SLD), with some pathologies also resembling the SLD subclassifications of metabolic dysfunction-associated steatotic liver disease (MASLD) and metabolic dysfunction-associated steatohepatitis (MASH). Specifically, TCDD induces steatosis (reversible hepatic fat accumulation) and immune cell infiltration, as reported in SLD [7–10]. Chronic exposure to TCDD also induces extracellular matrix (ECM) remodeling, leading to fibrosis, a pathology observed in advanced stages of MASH [8, 10, 11]. During liver disease progression, ECM remodeling can result in irreversible cirrhosis, which if unchecked, increases the risk for hepatocellular carcinoma (HCC) or end-stage liver disease requiring transplantation [12]. Interestingly, in a 2 year mouse carcinogenicity study, TCDD induced HCC [13]. TCDD also elicits hepatomegaly and bile duct proliferation [9, 14–16]. However, the underlying initial responses triggering TCDD-induced pathologies remain enigmatic. The similarities between TCDD-induced liver pathologies and SLD etiologies suggest common mechanisms may be used. Moreover, shared cell-specific gene expression changes may identify similar mechanistic strategies in the progression of steatosis to steatohepatitis with fibrosis.

In this study, single-nuclei RNA-sequencing (snRNA-seq) was used to assess initial cell-specific gene expression responses to TCDD within 72 h that could be tracked to subsequent phenotypic responses. Cell composition, differential gene expression analysis, and gene set enrichment analysis (GSEA) tools were integrated to further elucidate the initial hepatic effects of TCDD. Neutrophil levels within 72 h increased, while gene set enrichment analysis (GSEA) confirmed the disruption of carbohydrate, lipid, and protein metabolism by TCDD in various, but not all, cell types. Furthermore, TCDD induced expression of genes known to promote reactive oxygen species (ROS) as early as 2 h. Genes associated with dyslipidemia were predominantly dysregulated in hepatocytes, including those involved in fatty acid uptake and β-oxidation. TCDD disrupted retinol metabolism in HSCs consistent with the phenotypic evidence of fibrosis. This study provides initial cell-specific gene expression responses that underlie the hepatic effects of TCDD.

Results and discussion

Cell composition analysis

The UMAP shows 10 clusters following Leiden's analysis of snRNAseq data that were further characterized as specific cell types based on the expression of known marker genes (Fig. 1A and B, Figure S1, Table S1). As previously reported, hepatocytes were the most abundant cell type followed by endothelial cells (ECs), hepatic stellate cells (HSCs), macrophages, B cells, T cells, portal fibroblasts (PFs), cholangiocytes, plasmacytoid dendritic cells (pDCs), and neutrophils. Hepatocytes and pDCs represented the most (80.7%) and least (0.1%) abundant cell types, respectively (Fig. 1C). The relative proportions of hepatic cell types did not change following treatment with vehicle or TCDD the time course study, except for neutrophils, which increased at 72 h (Fig. 1D). This is consistent with neutrophils being the initial line of defense [17]. In addition, six EC subtypes (pericentral liver sinusoidal ECs [LSECs], midzonal LSECs, periportal LSECs, lymphatic ECs [LyECs], periportal vascular ECs [VECs], and pericentral VECs) were identified based on specific established markers [18]. A seventh EC cell subtype, dubbed proliferative ECs [PECs] was also identified based on the expression of *Cenpp*, *Top2a*, and *Mki67* (Figures S2A and 2B). PEC numbers increased ~ 4-fold at 72 h indicating EC proliferation (Figure S2C). Two macrophage subtypes (Kupffer cells [KCs] and monocyte-derived macrophages [MDMs]) were also identified using established cell markers [19] (Figures S3A and S3B), with no change in cell population following treatment (Figures S3C). Although no overt signs of inflammation were detected in histological sections within 72 h (Figure S4), previous studies have reported that TCDD induces the infiltration of macrophages, B cells, T cells, and neutrophils in mice following repeated treatments [20]. The results from the present study highlight the initial cell type changes in response to TCDD, with neutrophils

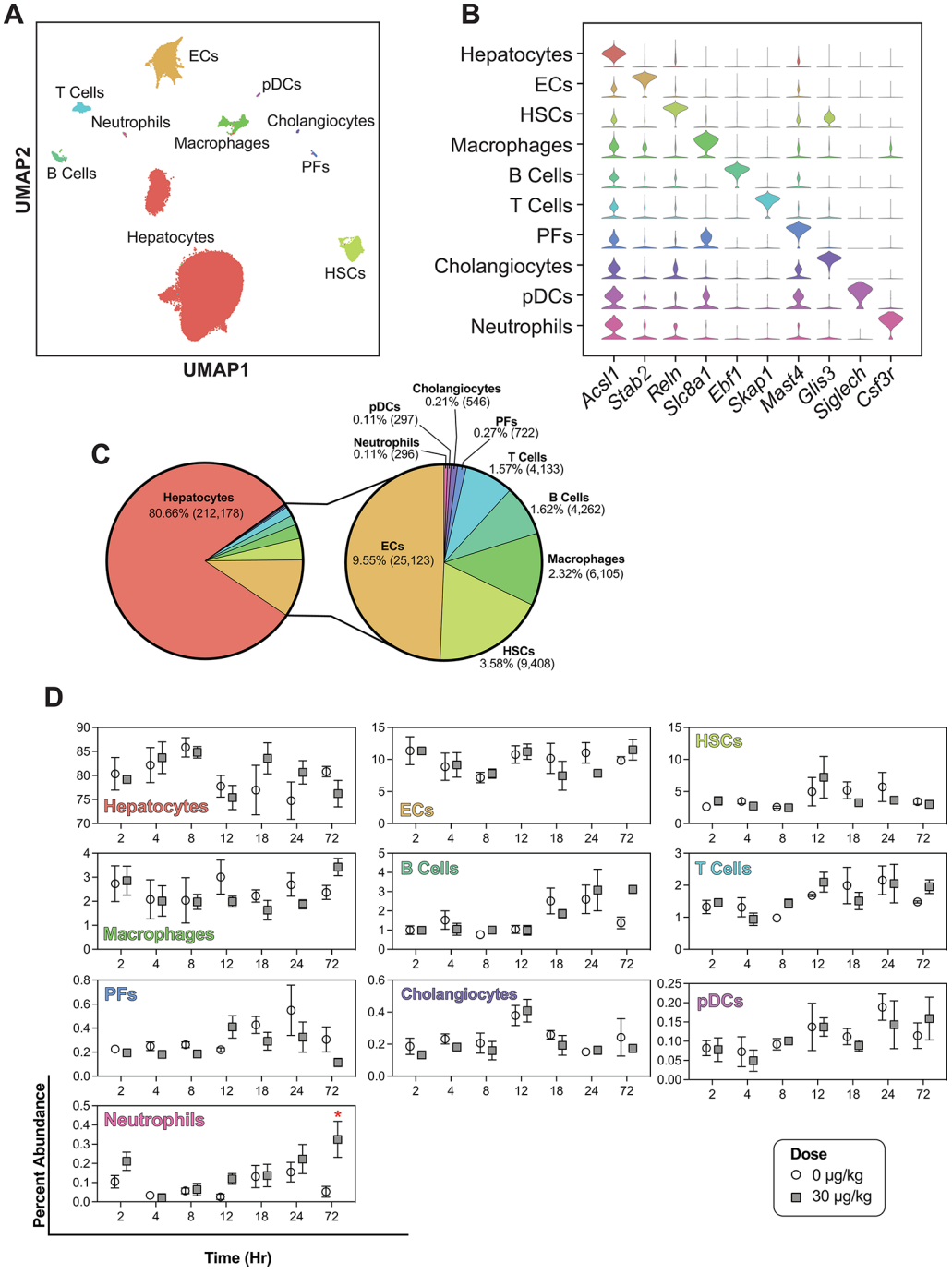

Fig. 1 Identification of distinct cell types in the liver. (**A**) UMAP visualization of cell types determined by Leiden clustering. (**B**) The expression of representative known markers used to further characterize cluster identity. (**C**) Relative proportions of ten identified cell types across all time points. (**D**) Relative abundance of specific cell types, calculated as a percentage of the total cells, at a specific time point. Plots depict mean ± SEM. Significance (*$p \leq 0.05$) was determined using a one-way ANOVA followed by Dunnett's post-hoc analysis

being the first immune response, with other leukocytes to follow.

Differential gene expression

Differential gene expression elicited by TCDD was assessed at 2, 4, 8, 12, 18, 24, or 72 h post-oral gavage with time-matched vehicle controls using snRNAseq. Cell-specific differentially expressed genes (DEGs) highlight the temporal dynamics and regulatory responses (Table S2). Top DEGs in most cell types included the AHR battery genes *Cyp1a1*, *Cyp1a2*, and *Ahrr* (Figure S5). Other genes such as *Cyp1b1* and *Nqo1*, as well as the predicted

AHR target *Xdh*, were induced at all time points in hepatocytes (Table S2). *Cyp1a1*, *Cyp1a2*, *Cyp1b1 and Xdh* are also known to produce reactive oxygen species (ROS) [21]. Neutrophils were unique in exhibiting no detectable DEGs, perhaps due to their low abundance (296 total neutrophils detected). Subsequent analyses focused on DEGs unique to each respective cell type as well as pathways relevant to induced pathologies.

Hepatocytes had a total of 4,785 DEGs, with 4,071 being specific to this cell type (Fig. 2). Of these, 71.6% possessed a pDRE with only 28.2% exhibiting genomic AHR binding in a published 2-hour ChIPseq dataset (Fig. 2) [7, 22]. Differential gene expression was greatest at 4 h with 77 genes consistently induced across all 7 time points (Figure S6). Only *Pklr*, the pyruvate kinase liver/erythrocyte isoform, was consistently repressed, as previously reported [23]. *Ecel1* was one of the most induced genes (Figure S7), and although the hepatic role of ECEL1 is unknown, other endothelin-converting enzymes are associated with fibrogenesis in other liver injury models [24]. *Nptx1*, encoding neuronal pentraxin 1, was also induced across all time points (711-fold at 12 h). Despite its known oncogenic role in various tumors, NPTX1 expression is protective in HCC by promoting apoptosis [25]. *Smcp* (435-fold at 4 h), encoding sperm mitochondria-associated cysteine-rich protein, also provides structural integrity during HCC development [26]. The carboxylesterase, *Ces1h*, was induced between 4 and 24 h with 123-fold induction at 4 h. Studies suggest CES1H mitigates liver disease, while others report it attenuates diet- and alcohol-induced steatohepatitis and hyperlipidemia [27]. Other CES isoforms, such as *Ces1b*, are also induced by TCDD [28]. The sulfotransferases *Sult2a1* (24.2-fold at 12 h), *Sult2a4* (129-fold at 12 h), *Sult2a5* (25.5-fold at 12 h), and *Sult3a1* (94.4-fold at 4 h) were repressed, and have been associated with liver disease [29]. Overall, several hepatocyte-specific DEGs were associated with liver function and disease, including fibrosis, oncogenesis, and metabolic regulation.

A total of 710 DEGs were identified in ECs with 226 being unique of which 81.0% possessed a pDRE and 45.1% exhibiting AHR genomic binding (Fig. 2). Sixteen DEGs were consistently induced across all time points (Figure S6), which included AHR battery genes as well as *Ackr3*. In preclinical models, *Ackr3* induction in LSECs mitigated liver fibrosis while possessing pre-regenerative properties [30]. *Fgf23*, which is typically associated with osteocyte expression and plays a role in the regulation of phosphate and vitamin D metabolism, was induced 77.0-fold at 12 h, making it the most induced EC gene (Figure S7). A meta-analysis of clinical studies found *Fgf23* to be the most induced LSEC gene in cirrhosis samples when compared to non-cirrhotic controls [31]. *Chst11*, a producer of the integral ECM component, heparan sulfate, was induced 10.3-fold at 4 h. Elevated CHST11 correlated with poor HCC survival [32]. Interestingly, *Sulf1*, a sulfatase involved in the removal 6-O-sulfate groups from various substrates, including heparan sulfate, was induced 8.6-fold at 12 h. In contrast, *Csmd1*, a tumor suppressor in diverse tissues, was repressed 9.1-fold at 12 h [33, 34]. Other repressed genes include *Plagl1* (3.5-fold at 12 h), a cell proliferation regulator [35], and *Hgf* (2.8-fold at 4 h), which encodes for hepatocyte growth factor.

Of the 373 unique HSC DEGs, 86 were unique with 91.9% and 46.5% having a pDRE and AHR

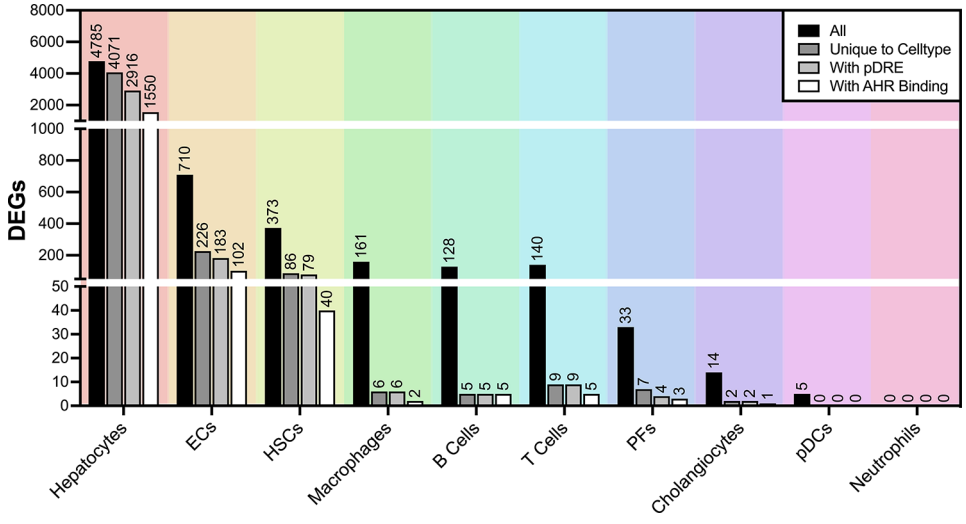

Fig. 2 Cell-specific differential gene expression in response to TCDD. Genes with a |fold-change| ≥ 1.5 and an adjusted p-value ≤ 0.05 were considered differentially expressed. The total number of DEGs across all time points (black), cell-specific DEGs in the respective cell type (dark gray), the number of unique genes that possessed a pDRE (light gray), and the number of unique genes that exhibited AHR genomic binding 2 h after TCDD treatment (white) are represented

binding, respectively. *Adgre4*, *Arap2*, *Bco1*, *Bend4*, *Cyp1a1*, *Cyp1a2*, *Frem2*, *Nfe2l2*, and *Tiparp* were induced across all time points (Figure S6). *Adgre4*, encodes for an EGF-TM7 receptor that attracts leukocytes, *Bco1* is involved in vitamin A metabolism [36], *Frem2* is a constituent of the basement membrane [37], and *Nfe2l2* encodes for NRF2, a transcription factor that is responsive to oxidative stress. Quiescent HSCs are a reservoir for vitamin A, while disruptions in vitamin A metabolism affecting antioxidant processes and retinoid signaling in SLD [38, 39]. Three uncharacterized genes, *A730004F24Rik*, *Gm31333*, and *C730002L08Rik* were also highly induced (Figure S7). *Frem2* was induced 50.6-fold at 72 h while *Per1*, a circadian regulator was induced 14.8-fold at 72 h with AHR genomic binding. Conversely, *Agxt* which metabolizes glyoxylate to glycine, was repressed 5.4-fold in HSCs at 12 h. Repression of *Agxt* repression due to DNA hypermethylation has been reported in mice with MASLD-like pathologies [40]. *Hpse2* (3.2-fold) and *Col25a1* (2.4-fold), are both ECM constituents. *Heyl*, a downstream target of NOTCH signaling implicated in liver development and regeneration [41], was repressed 2.8-fold repression at 18 h as was *Skil* (2.4-fold), a negative regulator of TGF-β signaling [42].

TCDD elicited 161 DEGs in macrophages. Six induced genes were unique, with each possessing a pDRE but only two having AHR binding (Fig. 2). Only *Cyp1a1*, *Cyp1a2*, *Selenbp1*, *Tiparp*, and *Xdh* were induced across all time points (Figure S6). *St18* which regulates the cell cycle and is associated with HCC [43], was induced 55.5-fold at 4 h and 63.1-fold at 12 h (Figure S7). *Amz1*, an M2 macrophage differentiation marker [44], was induced 3.8- and 2.6-fold at 4 and 72 h, respectively. *Mgat4a* (induced 3.5-fold at 4 h) catalyzes β1,4-N-acetylglucosamine (GlcNAc) glycosylation which distinguish macrophages subpopulations [45]. *Tifab*, a monocyte marker that regulates inflammatory pathways [46], was induced 3.2-fold at 2 h. *Tbxas1* and *Usp12*, which were induced 2.5- and 1.9-fold, respectively, contribute to thromboxane biosynthesis and protein deubiquitylation processes, respectively. While few markers of pro-inflammation were detected prior to 72-hours in the current study, notable immune cell accumulation is reported at 168 h following TCDD treatment [47].

Of 128 B cell DEGs, 5 were unique with one being induced (*Shroom2*) and four repressed (*St3gal5*, *Esr1*, *Asl*, and *Scp2*). Each contained a pDRE and exhibited AHR binding (Fig. 2). *Cyp1a1*, *Cyp1a2*, *Htatip2*, and *Selenbp1* were differentially induced across all time points (Figure S6). *Htatip2* is reported to suppress hepatic carcinogenesis [48], while *Shroom2* (2.6-fold at 18 h), the lone-induced B cell gene, has a cytoskeletal structure function in ECs [49] (Figure S7). Conversely, *St3gal5* and *Esr1* were repressed 2.8- and 3.0-fold, respectively, at 12 h. *Esr1*, which encodes estrogen receptor α, protects against HCC [50]. At 24 h, *Asl*, which hydrolyses argininosuccinate into arginine and fumarate, and was repressed, corroborating the repression of the urea cycle by TCDD [51]. *Scp2*, which encodes sterol carrier protein, was also repressed 3.9-fold at 4 h, a phenomenon previously observed in mice treated with TCDD [28].

T Cells are pivotal players in inflammation associated with liver disease progression. Seven differentially induced (*Asb2*, *Apex2*, *Acad11*, *Tecm Cped1*, *Zswim6*, and *Ppm1h*) and 2 repressed (*Itgal* and *Sntb2*) genes were unique to T cells with *Asb2*, *Cyp1a1*, *Cyp1a2*, *Selenbp1*, and *Tiparp* induced across all time points (Fig. 2, B). *Asb2* showed AHR binding and persistent induction (max 4.2-fold at 2 h) across all time points potentially contributing to protein degradation pathways (Figure S7). *Apex2*, a DNA repair factor combating oxidative stress, was induced 2.9-fold at 12 h, and is an HCC marker [52]. *Acad11*, induced 2.6-fold at 4 h with AHR binding, contributes to fatty acid metabolism, and *Tec*, which had AHR binding and was induced 2.5-fold at 2, mediates T cell differentiation [53]. *Cped1*, *Zswim6*, and *Ppm1h* were all induced at 4 h (2.1-, 1.9-, and 1.8-fold, respectively), and participate in protein processing, protein-protein interactions, and dephosphorylation regulatory mechanisms, respectively. Notably, PPM1H protects against HCC [54]. *Itgal* and *Sntb2* were the only repressed genes at 12 and 4 h respectively. ITGAL (a.k.a. CD11a) is a pan-leukocyte marker that plays a role in inflammatory responses [55].

PFs serve a crucial role in response to liver injury and disease. In total, 33 PF DEGs were identified with *Klf13*, *Acnat1*, *Rian*, *Cyp2c29*, *Pdpn*, *Nrg2*, and *Pkhd1l1* being unique. Only *Cyp1a2* was induced across all time points (Fig. 2). *Klf13* (6.7-fold induction at 2 h), encodes the KLF13 transcription factor that regulates cell proliferation in MASLD [56] and HCC [57], and had AHR binding. *Acnat1*, which encodes a peroxisomal acyl transferase, also showed AHR binding and was induced at 4 h (5.8-fold), underscoring a potential early role in the disruption of lipid metabolism. Non-coding *Rian* was induced at 2 h which promotes HCC in mice when overexpressed [58]. *Cyp2c29* was induced 4.6-fold at 24 h and protects against inflammation in mouse liver injury models induced by acetaminophen and carbon tetrachloride [59]. *Nrg2* (encoding neuregulin 2) showed AHR genomic binding and was induced 2.7-fold at 2 h, and is elevated in HCC [60]. Other neuregulins, such as NRG1, are also dysregulated by TCDD [61]. *Pkhd1l1*, which encodes for polycystic kidney and hepatic disease 1, was the only repressed PF gene (5.8-fold at 8 h).

Of the 14 unique cholangiocyte DEGs, non-coding 2610035D17Rik, and the GLIS Family Zinc Finger 3 (*Glis3*) were the only unique genes, both of which were

induced (Fig. 2). Mutated *Glis3* is implicated in liver disease particularly in abnormal bile duct development in pediatric cirrhosis [62]. *Glis3* possessed pDREs and AHR binding (Figure S7).

Although 5 DEGs were identified in pDCs, none were unique, and no DEGs were identified in neutrophils.

Gene set enrichment analysis

GSEA identified the disruption of metabolic function in specific cell types (Fig. 3, Table S3). This included xenobiotic metabolism, protein processing, carbohydrate, lipid, amino acid, vitamin, one carbon, retinol, and glutathione metabolism, as well as pathways pertaining to cell signaling and transport.

Several gene sets related to TCDD-mediated AHR signaling were over-represented, including cytochrome P450 (CYP450) in all cell types except for pDCs. *Cyp1a2*, a known AHR battery gene, as well as *Fmo3*, were the only xenobiotic metabolism genes enriched in every cell types. *Fmo3* induction is a known TCDD responsive gene [63], with hepatic induction associated with gut dysbiosis and glucose dysregulation [64]. Other common DEGs in most cell types included *Aox1*, *Gstm1*, *Gstp2*, *Cyp2a5*, and *Fmo1*.

Pathways related to carbohydrate, lipid, and protein metabolism, were enriched. In macrophages and PFs, starch and sucrose metabolism were over-represented. *Ugdh* and *Gbe1* were common in both cell types, while macrophages also displayed enrichment for glucuronosyltransferases (UGTs). UDP-glucose-6-dehydrogenase (*Ugdh)* which converts UDP-glucose to UDP-glucuronate mitigates NASH development by inhibiting RIPK1 kinase-dependent hepatocyte apoptosis [65]. *Gbe1* encodes glycogen branching enzyme, which is increased in high-fat diet mouse obesity models [66]. Interconversion of glucuronate and pentose, a five-carbon sugar intermediate essential for nucleic acid biosynthesis, was enriched in hepatocytes, macrophages, and B cells. Ten UGTs were induced in hepatocytes, all of which convert UDP-D-glucuronate to D-glucuronosides, required for conjugation catalyzed by Phase II enzymes. UGT induction by TCDD involves nuclear factor (erythroid-derived 2)-like 2 (NRF2), a pivotal regulator of oxidative stress [67].

Lipid dysregulation was also identified by GSEA. Steroid metabolism was perturbed in hepatocytes, macrophages, B cells, and T cells with the enrichment of CYP450 and UGT genes, which also function in xenobiotic metabolism. In addition, these 4 cell types were enriched for *Hsd17b6*, a hydroxysteroid dehydrogenase, and HCC prognostic biomarker that correlates with infiltrating leukocytes [68]. Hepatocytes were also enriched for steroid 5α-reductases (*Srd5a1* and *Srd5a2*), which are involved in steroid metabolism including

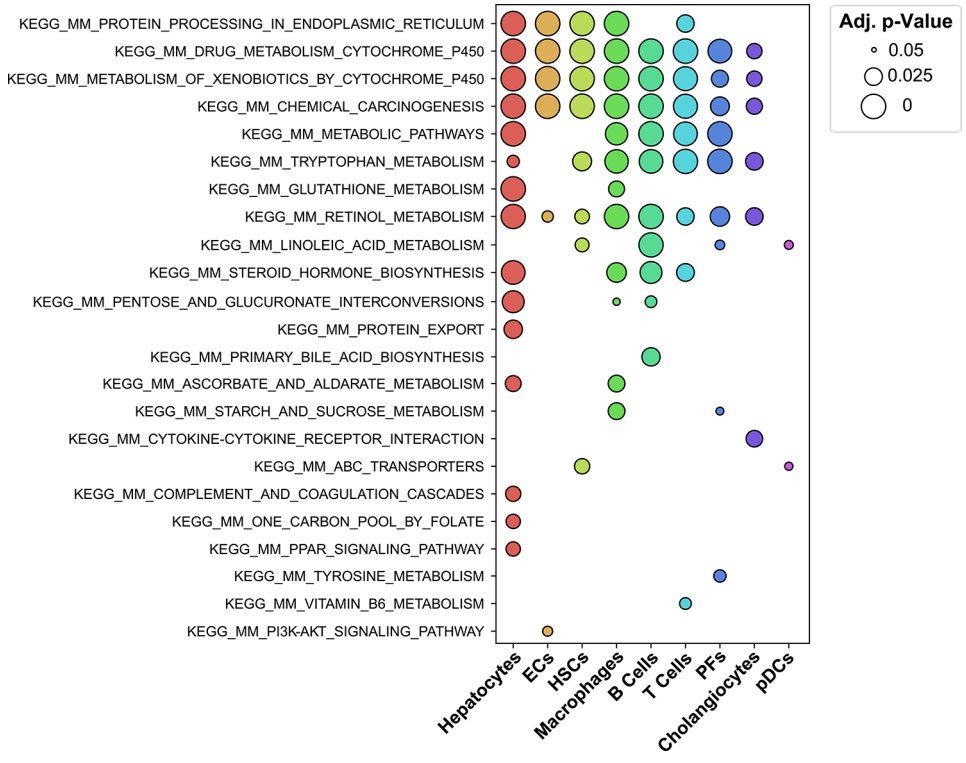

Fig. 3 Gene set enrichment analysis for each cell type. Total DEGs for each cell type were assessed for enriched KEGG pathways. Enrichment with an adjusted p-value ≤ 0.05 was considered significant. The dot size represents the adjusted p-value

the interconversion of testosterone to the more potent dihydrotestosterone. Inhibition of *Srd5a1* and *Srd5a2* is linked to hepatic lipid accumulation in humans [69]. Moreover, the metabolism of linoleic acid was impacted in HSCs, B cells, PFs, and pDCs. Genes in this term overlapped with xenobiotic metabolic responses including CYP450 and aldo-keto reductase genes. Lastly, primary bile acid synthesis was enriched in B cells. *Scp2*, encoding sterol carrier protein 2, was enriched and associated with hepatic steatosis and SLD pathogenesis [70]. In addition, *Acox2*, encoding acyl-CoA oxidase 2, was enriched. Inborn errors in *Acox2* have been attributed to hepatotoxicity due to bile acid intermediate accumulation that contributes to fibrosis [71]. *Cd36*, a fatty acid translocase was induced by TCDD at 4, 18, and 72 h in hepatocytes (Table S2). *Cd36* induction by TCDD correlates with steatosis [47, 72, 73], while its knockout mitigates TCDD induced steatosis [72]. Hepatocytes also exhibited the repression of acyl-CoA synthetases *Acsl3*, *Acsl4*, and *Slc27a3* across various time points, which are responsible for the activation of long- and very long-chain fatty acids prior to β-oxidation. This was accompanied by suppression of *Tm6sf2* at 4, 18, and 72 h, and the induction of *Angptl3* at 2, 4, 12, and 18 h. Histological assessment indicated that these transcriptional changes in lipid metabolism are sufficient to induce the accumulation of lipids in the liver as denoted by ORO staining within 72 h (Figure S4). Together, these gene expression and histological changes are consistent with prior studies that reported TCDD induced lipid mobilization as early as 24 h after treatment [47].

GSEA suggested all cell types, except ECs, were enriched in tryptophan metabolism [74–77]. All but cholangiocytes differentially expressed *Tdo2*, which encodes for tryptophan 2,3-dioxygenase, the rate-limiting enzyme for tryptophan catabolism. TDO2 also promotes HCC proliferation due to interleukin (IL)-6-induced tumor cell proliferation [78]. In PFs, TCDD also disrupted aromatic L-amino acid decarboxylase (*Ddc*) which is involved in tyrosine metabolism. DDC produces several neurotransmitters, including tyramine from tyrosine, tryptamine from tryptophan, and histamine from histidine.

DEGs associated with protein processing and transport were overrepresented. ATP-binding cassette (ABC) transporters were enriched in HSCs. Protein export was dysregulated in hepatocytes, while processing events were enriched in hepatocytes, ECs, HSCs, macrophages, and T cells. *Nfe2l2*, which encodes for NRF2, was enriched in all 5 cell types with *Hyou1* (hypoxia up-regulated protein 1). Moreover, *Hspa5* (heat shock protein family A member 5) was enriched in the six cell types. HSPA5 serves as an ER chaperone and is a key alternative splicing regulator for SLD-related genes [79]. Interestingly, TCDD is reported to promote ER stress in vitro, implicating protein processing events [80].

Glutathione metabolism was overrepresented in both hepatocytes and macrophages. The catalytic subunit of glutamate-cysteine ligase, *Gclc*, which is responsible for glutathione synthesis, was not only induced hepatocytes and macrophages, but also ECs, HSCs, B cells, T cells, and PFs, all at 4 h. Hepatocyte-specific GCLC knockout exacerbates liver injury, steatosis, and inflammation, concurrent with compromised mitochondrial function [81]. *Gclc* induction may be response to accumulating oxidative stress due to the induction of *Cyp1a1*, *Cyp1a2*, *Cyp1b1* and *Xdh* as early as 2 h (Table S2).

All cells except pDCs were enriched for retinol metabolism. Quiescent HSCs serve as the largest store of vitamin A [82]. Seven genes associated with retinol metabolism in HSCs were induced including *Hsd17b6* and *Aox1* (Table S2). *Hsd17b6* metabolizes retinol into its more biologically active form, retinal, whereas *Aox1* converts retinal into retinoic acid, the protoypical ligand for retinoic acid receptor (RAR) and retinoid X receptor (RXR) activation [83]. Subsequently, retinoic acid is further metabolized into more water-soluble hydroxy- and oxo-forms by CYP450 enzymes, including *Cyp1a1*, *Cyp2a5*, *Cyp1b1*, *Cyp2c37*, and *Cyp2c50* that are induced in HSCs by TCDD. Early induction of retinol metabolism genes, including the conversion cascade from retinol to retinoic acid, underscore their role as indicators of hepatic stellate cell activation.

DEGs related to PI3-AKT signaling in ECs including *Kit* and *Kitl* were induced as early as 2 h (2.1- and 2.8-fold, respectively) suggested enrichment of cell signaling and interaction pathways. Activation of KIT, a key regulator of cell proliferation, is consistent with EC proliferation [84]. There was also enrichment of metabolism of vitamin B6 in T cells, as well as ascorbate and aldarate in hepatocytes and macrophages. One-carbon metabolism (OCM) was also disruption by TCDD as previously reported [85]. In total, 12 of 18 OCM genes were differentially expressed in hepatocytes.

When assessing enriched complement and coagulation genes in hepatocytes, *Serpine1* was induced across all time points (max induction 705-fold at 2 h). *Serpine1* encodes plasminogen activator inhibitor 1 (PAI-1) and inhibits uPA (urokinase-type plasminogen activator) and tPA (tissue-type plasminogen activator), both plasminogen activators. uPA and tPA are serine proteases that convert plasminogen into plasmin, and maintain ECM homeostasis [86]. *Plg* (encoding plasminogen) repression at 2 and 12 h in hepatocytes, in conjunction with increased *Serpine1* levels, suggests conditions favoring ECM accumulation, and the development of fibrosis [86].

Collectively, GSEA identified overrepresented gene expression changes associated with SLD-related

pathologies such as steatosis, inflammation, and fibrosis, as well as HCC, and identified specific cell types that contribute to these responses.

Conclusion

TCDD induces a spectrum of SLD-related pathologies, including steatosis, inflammation, and fibrosis, in addition to disrupting/promoting cell proliferation. Single-nuclei analysis of liver cell subtypes following a single oral gavage of TCDD identified early cell-specific gene expression responses and a cacophony of cell-cell interactions.

SLD development and progression to more severe disease such as MASH is driven by a multi-hit process that is often fueled by heightened oxidative stress. Although the exact origin of TCDD-induced ROS remains unknown, the induction of oxidative metabolism pertaining to *Cyp1a1*, *1a2*, *1b1*, *Nqo1*, and *Xdh*, are likely sources. At later timepoints (>18 h), when TCDD has induced hepatic fat accumulation, oxidative stress would be further exacerbated due to the lipid peroxidation. Results from this study suggest that oxidative stress was induced in hepatocytes, ECs, HSCs, and macrophages as early as 2 h based on the induction of NRF2 (*Nfe2l2*), the quintessential sensor of oxidative stress. In response, ten glutathione S-transferases (GSTs) were induced in hepatocytes with *Gstp1* and *Gstp2* induced by 2 h and the remaining eight induced by 4 h. These results are consistent with the bulk RNAseq data where *Gstp1* and *Gstp2* induction occurred within 4 h after TCDD treatment. GSTPs serve a defense role by conjugating glutathione (GSH) to reactive oxygen species (ROS) and lipid peroxides (LOS) to facilitate detoxification and excretion. *Nqo1* and *Esrrg*, genes encoding NAD(P)H quinone dehydrogenase 1 and estrogen-related receptor γ, respectively, are members of the NRF2 target gene battery that are induced in response to oxidative stress. The early induction of *Nqo1* (2 h) and *Esrrg* (4 h) in hepatocytes provides further evidence of oxidative stress in TCDD-treated livers, contributing to the advancement of SLD pathologies. These findings highlight a probable mechanism in which oxidative stress and lipid accumulation catalyze downstream pathologies such as inflammation.

Hepatic fat accumulation is one of the first phenotypic effects of TCDD which is reported as early as 72 h following exposure, resulting from the induction of lipid uptake coupled with peripheral fat mobilization, the repression of β-oxidation and impaired lipoprotein assembly and export. Hepatocytes are the primary site of dyslipidemia following the early induction of *Cd36*, which facilitates fatty acid uptake. Moreover, hepatocytes exhibited repression of acyl-CoA synthetases, crucial for long-chain fatty acid activation and subsequent β-oxidation, the suppression of *Tm6sf2*, and the induction of *Angptl3*, all of which are consistent with triglyceride accumulation. GSEA also identified the disruption of steroid (vis-à-vis cholesterol) metabolism in hepatocytes, macrophages, B cells, and T cell. In addition, perturbations in linoleic acid metabolism emerged as a notable feature, affecting HSCs, B cells, PFs, and pDCs. Collectively, these results underscore the initial cell-specific effects and interactions involved in hepatotoxicity and the progression of steatosis to steatohepatitis with fibrosis, pathologies that mirror aspects of SLD progression.

Previous studies have reported the onset of immune cell infiltration following oral gavage with 30 μg/kg TCDD at 168 h. Although a notable influx of neutrophils was detected at 72-hours, no indication of other immune responses, such as macrophage recruitment were noted. Therefore, the 72-hour duration in our study appears to be insufficient for the manifestation of such immune cell infiltration, in contrast to 28 day studies.

Despite a lack of evidence for acute inflammatory responses, differential gene expression pertaining to ECM remodeling and fibrogenesis was observed. HSCs exhibited DEGs related to the interconversion of retinol to the more biologically active retinal, retinoic acid, and the related metabolites, a hallmark of HSC activation. Activated HSCs remodel ECM and promote the accumulation of pro-fibrotic proteins such as collagens, fibronectins, elastins, laminins, hyaluronans, and proteoglycans. Furthermore, the early induction of endothelin-converting enzyme *Ecel1* in hepatocytes, and *Ackr3* in ECs, may mitigate fibrogenesis. The induction of *Serpine1* in hepatocytes would inhibit uPA and tPA, thereby keeping fibrinolysis in check. In parallel, *Plg* repression in hepatocytes would reduce plasmin and attenuate ECM degradation. These gene expression changes may represent the initial activation of fibrogenesis in HSCs, as well as the compensatory responses by hepatocytes.

TCDD clearly disrupted regulatory mechanisms governing cell proliferation, with potential implications for HCC development. For instance, at all timepoints hepatocytes exhibited the upregulation of *Nptx1*, known to confer protection against HCC progression, and *Smcp*, which conversely is associated with promoting HCC. Concurrently, ECs show increased expression of *Chst11*, an HCC marker of poor prognosis, while the repression of the tumor suppressor gene *Csmd1* in hepatocytes may further promote proliferation. The induction of neuregulin genes, *Nrg1* and *Nrg2*, across various cell types including hepatocytes, PFs, and pDCs, highlights a potential role in HCC pathogenesis. The proliferation of PECs may be due to HSC-mediated *Vegfc* signaling through receptors, *Kdr* and *Flt4*, on ECs, a pathway known to support cellular proliferation. Furthermore, the induction of *Igf* in cholangiocytes emerges as a novel contributor to hepatocyte proliferation. This suggests interactions between

liver cell types represent underlying mechanisms associated with cell proliferation and the development of TCDD-induced HCC.

In conclusion, this study reveals the complex effects of TCDD on early gene expression in specific cell types that contribute to SLD-related pathologies. It examines cell-specific gene expression responses, the induction of oxidative stress, lipid metabolism disruption, and the early stages of fibrogenesis. snRNAseq analysis has identified disrupted pathways and cell-cell interactions that further elucidate the roles of specific cell types in the progression of steatosis to steatohepatitis with fibrosis. The mapping of initial cell specific responses to TCDD, not only advances our mechanistic understanding of toxicant-induced liver pathologies but also sets the stage for future investigations aimed at mitigating the adverse effects of environmental contaminants on liver function and overall health.

Methods

Animal treatment

Male C57BL/6Crl mice were received from Charles Rivers Laboratories (Wilmington, MA) at postnatal day (PND) 25 and housed in Innocages (Innovive, San Diego, CA) with ALPHA-dri bedding (Shepherd Specialty Papers, Chicago, IL). The mice were provided Harlan Teklad 22/5 Rodent Diet 8940 (Envigo, Indianapolis, IN) and Aquavive water (Innovive) *ad libitum*. On PND 28, the mice were orally gavaged at Zeitgeber time (ZT) 00 with sesame oil vehicle (Sigma-Aldrich, St Louis, MO), or 30 μg/kg TCDD (AccuStandard, New Haven, CT). At intervals of 2, 4, 8, 12, 18, 24, and 72 h (corresponding to ZT 02, 04, 08, 12, 18, 00, and 12, respectively), the mice were euthanized by carbon dioxide asphyxiation with subsequent cardiac puncture, and liver samples were collected, snap-frozen, and stored at -80 °C. The study used male mice only, following previous reports indicating similar hepatic pathologies in both sexes, with males exhibiting greater sensitivity [7]. All procedures were approved by the Michigan State University Institutional Animal Care and Use Committee, adhering to ARRIVE guidelines [87].

Single-nuclei library preparation and sequencing

Three biological replicates were used for each dose and time-point. A previously used protocol was to extract nuclei (https://doi.org/10.17504/protocols.io.3fkgjkw). Briefly, approximately 100–300 mg of frozen liver was placed in a disposable Dounce homogenization tube and cut into small pieces. Then, 500 μL of 4 °C nuclei EZ lysis buffer (MilleporeSigma, Burlington, MA) was added, and the tissue was homogenized using a disposable pestle. Next, ~900 μL of Nuclei EZ lysis buffer was added, and the mixture was incubated on ice for 5 min, gently inverting a few times during the incubation. The homogenate was passed through a 70 μm strainer into a 50 mL conical tube using a wide bore pipette tip. The flow-through was transferred to a 2 mL tube and centrifuged at 4 °C for 5 min at 500 g. The supernatant was discarded, after which the pellet was gently resuspended in 1.5 mL EZ lysis buffer and incubated on ice for 5 min. The nuclei were re-centrifuged at 4 °C for 5 min at 500 g. The supernatant was discarded, and the pellet was rinsed with 500 μL of nuclei wash and resuspension buffer (1X phosphate-buffered saline, 1% bovine serum albumin, 0.2 U/μL RNase inhibitor), taking care not to disturb the pellet, and allowed to rest on ice for 5 min. An additional 1000 μL of nuclei wash and resuspension buffer was added, and the nuclei were resuspended using a wide bore tip. The nuclei were centrifuged again at 4 °C for 5 min at 500 g, and the supernatant was discarded, leaving approximately 50 μL. The nuclei were gently resuspended in 1400 μL of nuclei wash and resuspension buffer. Again, the nuclei were centrifuged at 4 °C for 5 min at 500 g, and the supernatant was discarded, leaving approximately 50 μL. Finally, the nuclei were gently resuspended in 500 μL of DAPI nuclei wash and resuspend buffer (1X nuclei wash and resuspension buffer, 10 μg/mL DAPI) and filtered using a 40 μm strainer. The resuspended nuclei immediately underwent fluorescence-activated cell sorting using a BD FACSAria IIu cell sorter (BD Biosciences, San Jose, California) with a 70-μm nozzle at the MSU Flow Cytometry Core Facility (https://facs.iq.msu.edu, last accessed November 2, 2023).

Libraries were prepared using the 10x Genomics Chromium Single Cell 3′ v3.1 kit in conjunction with the 10X Genomics Dual Index kit (10X Genomics, Pleasanton, CA; protocol revision CG000315 Rev A), then submitted for 150-bp paired-end sequencing at a depth ≥ 50,000 reads/cell using the NovaSeq 6000 at Novogene (Beijing, China). The alignment of reads was performed using Cellranger 4.0.0 (10X Genomics) to a custom reference genome (mouse mm10 release 93 genome build), which accounted for both introns and exons to capture pre-mRNA and mature mRNA within the nuclei. Aligned reads were further filtered to include only (i) cells with a minimum of 100 genes, (ii) genes that were recognized in a minimum of 3 cells, and (iii) cells with ≤ 1% mitochondrial DNA. Scrublet v0.2.3 was used to remove putative doublets [88].

Cell identification

To integrate all libraries together prior to clustering, Scanpy v1.9.3 was used to determine the 2,000 most highly variable genes (HVGs) amongst all libraries [89]. These HVGs were used to integrate all libraries together using scVI v0.20.3, while accounting for dose and time as categorical covariates and using a latent variable of 40.

Leiden clustering was performed at varying resolutions (0.05, 0.1, 0.25, 0.5, 0.75, and 1.25). A resolution of 0.05 was selected to preserve the integrity of the parenchymal hepatocytes, while allowing for sub-clustering of less abundant cell types. At this resolution, 6 main clusters were identified, with cluster 3 exhibiting a high concentration of marker genes associated with immunological functions. This immunological cluster was subset for further analysis, to distinguish immunological cell subtypes. Using the 2,000 most HVGs, followed by Leiden clustering, 5 distinct clusters were identified at a resolution of 0.1. Marker genes, as determined by a Wilcoxon rank-sum test, for these clusters were used to identify B cells, macrophages, neutrophils, T cells, and plasmacytoid dendritic cells (pDCs). These cell annotations were integrated into the full dataset, after which any remaining unknown clusters at a resolution of 0.5 were identified also using a Wilcoxon rank-sum test to determine cell marker genes. In total, 10 cell types were identified in this dataset: B cells, cholangiocytes, hepatocytes, hepatic stellate cells (HSCs), endothelial cells (ECs), macrophages, neutrophils, pDCs, portal fibroblasts (PFs), and T cells. ECs and macrophages were subset to assess subpopulations, using previously published marker genes [18, 19]. Within the macrophage dataset, the analysis revealed monocyte-derived macrophages and Kupffer cells. Meanwhile, in the EC dataset, various subpopulations were identified, including pericentral liver sinusoidal ECs (LSECs), midzonal LSECs, periportal LSECs, lymphatic endothelial cells (LyECs), proliferating endothelial cells (PECs), periportal vascular endothelial cells (VECs), and pericentral VECs.

Differential gene expression analysis

A recent study demonstrated that differential gene expression analysis performed on pseudobulk data outperformed single-cell differential gene expression methods since the latter is biased towards highly expressed genes [90]. For this reason, gene expression for each cell type, at each dose and time-point, was pseudobulked for each biological replicate using Scater v1.22.0 before differential gene expression analysis [91]. Differential expression analysis was then performed using Deseq2 v1.34.0 [92] on time-matched groups between vehicle and TCDD treatment. Genes possessing a |fold-change| ≥ 1.5 and an adjusted p-value≤ 0.05 were considered differentially expressed in response to TCDD treatment.

Gene set enrichment analysis

Gene set enrichment analysis (GSEA) was performed using GSEApy v1.0.4 [93], using a custom list of gene sets that have previously been published (https://doi.org/10.7910/DVN/OCKYFO) [94]. Briefly, this list of gene sets includes those curated through the gene set knowledge base (GSKB) [95], as well as gene sets curated in-house.

Declaration of generative AI use

This manuscript has been enhanced for clarity and conciseness with the aid of OpenAI's ChatGPT-4. The authors reviewed and refined the output from the language model, ensuring the integrity and accuracy of the content. Responsibility for the final publication rests entirely with the authors.

Abbreviations

ARNT	AHR nuclear translocator
AHR	Aryl hydrocarbon receptor
ABC	ATP-binding cassette
GlcNAc	β1,4-N-acetylglucosamine
CYP450	Biphenyls (PCBs); cytochrome P450
DREs	Dioxin response elements
PCDFs	Dibenzofurans
DEGs	Differentially expressed genes
ECs	Endothelial cells
ECM	Extracellular matrix
GSEA	Gene set enrichment analysis
GSKB	Gene set knowledge base
UGTs	glucuronosyltransferases
GSH	Glutathione
GSTs	Glutathione S-transferases
H&E	Hematoxylin and eosin
HCC	Hepatocellular carcinoma
HSCs	Hepatic stellate cells
KCs	Kupffer cells
LSECs	Liver sinusoidal ECs
LyECs	Lymphatic ECs
MASLD	Metabolic dysfunction-associated steatotic liver disease
MASH	Metabolic dysfunction-associated steatohepatitis
MDMs	Monocyte-derived macrophages
NRF2	Nuclear factor (erythroid-derived 2)-like 2
ORO	Oil red O
PAI-1	Plasminogen activator inhibitor 1
pDCs	Plasmacytoid dendritic cells
PCDDs	Polychlorinated dibenzo-p-dioxins
PND	Portal fibroblasts (PFs); postnatal day
SLD	Steatotic liver disease
snRNAseq	single-nuclei RNA-sequencing
TCDD	2,3,7,8-tetrachlorodibenzo-p-dioxin
TES	Transcription end site
TSS	Transcription start site
VECs	Vascular ECs
ZT	Zeitgeber time

Supplementary Information

The online version contains supplementary material available at https://doi.org/10.1186/s12864-024-10730-3.

Supplementary Material 1

Supplementary Material 2

Supplementary Material 3

Supplementary Material 4

Acknowledgements

Not applicable.

Author contributions
G.N.C. and T.Z. designed the project. G.N.C and R.N. conducted the animal study. G.N.C. performed the experiments. G.N.C. and R.N. developed the transcriptomics workflow. G.N.C. compiled all the data and produced the figures and tables. G.N.C. wrote the first draft of the manuscript. All authors reviewed and edited the manuscript.

Funding
This project was supported by the National Institute of Environmental Health Sciences (NIEHS) Superfund Research Program [NIEHS SRP P42ES004911] and the NIEHS Research Project Grant Program [NIEHS R01ES029541] to T.Z. Partial support to T.Z. was provided by AgBioResearch at Michigan State University. GNC was supported by NIEHS Multidisciplinary Training in Environmental Toxicology [T32ES007255].

Data availability
The datasets utilized in this manuscript are all accessible to the public following the guiding principles of Findable, Accessible, Interoperable, and Reusable (FAIR) data. The code utilized in this study has been made readily accessible to enhance reproducibility (https://github.com/zacharewskilab/publication_analyses/tree/main/Analyses/TC_TCDD_snRNAseq). Raw snRNAseq data has been deposited in the Gene Expression Omnibus (GSE254121) Processed data has been deposited on the Broad Single Cell Portal (SCP2482). Data from AHR ChIP-seq (GSE97634) and the computationally detected potential dioxin response elements (pDREs, https://doi.org/10.7910/DVN/JASCVZ) have been previously published [97]. The ChIP-seq analysis employed a false discovery rate (FDR) threshold of ≤ 0.05. pDREs were deemed functional if they had a matrix similarity score (MSS) of ≥ 0.856 and were associated with genes situated within a range of 10 kb upstream of the transcription start site (TSS) to the transcription end site (TES).

Declarations

Competing interests
The authors declare no competing interests.

Ethics approval
All procedures involving mice were conducted in accordance with the guidelines set forth by the Michigan State University Institutional Animal Care and Use Committee (PROTO202100219).

Consent for publication -
Not applicable.

Received: 8 May 2024 / Accepted: 21 August 2024
Published online: 28 August 2024

References

1. Larigot L, Juricek L, Dairou J, Coumoul X. AhR signaling pathways and regulatory functions. Biochim Open. 2018;7:1–9.
2. Suskind RR. Chloracne, the hallmark of dioxin intoxication. Scand J Work Environ Health. 1985;11(3 Spec No):165–71.
3. Kerkvliet NI. Recent advances in understanding the mechanisms of TCDD immunotoxicity. Int Immunopharmacol. 2002;2(2–3):277–91.
4. Eskenazi B, Ames J, Rauch S, Signorini S, Brambilla P, Mocarelli P, Siracusa C, Holland N, Warner M. Dioxin exposure associated with fecundability and infertility in mothers and daughters of Seveso, Italy. Hum Reprod. 2021;36(3):794–807.
5. Klaunig JE, Li X, Wang Z. Role of xenobiotics in the induction and progression of fatty liver disease. Toxicol Res (Camb). 2018;7(4):664–80.
6. Fernandez-Salguero PM, Hilbert DM, Rudikoff S, Ward JM, Gonzalez FJ. Aryl-hydrocarbon receptor-deficient mice are resistant to 2,3,7,8-tetrachlorodibenzo-p-dioxin-induced toxicity. Toxicol Appl Pharmacol. 1996;140(1):173–9.
7. Fader KA, Nault R, Zhang C, Kumagai K, Harkema JR, Zacharewski TR. 2,3,7,8-Tetrachlorodibenzo-p-dioxin (TCDD)-elicited effects on bile acid homeostasis: alterations in biosynthesis, enterohepatic circulation, and microbial metabolism. Sci Rep. 2017;7(1):5921.
8. Nault R, Fader KA, Ammendolia DA, Dornbos P, Potter D, Sharratt B, Kumagai K, Harkema JR, Lunt SY, Matthews J, et al. Dose-dependent metabolic reprogramming and Differential Gene expression in TCDD-Elicited hepatic fibrosis. Toxicol Sci. 2016;154(2):253–66.
9. Nault R, Fader KA, Kopec AK, Harkema JR, Zacharewski TR, Luyendyk JP. From the cover: coagulation-driven hepatic fibrosis requires protease activated Receptor-1 (PAR-1) in a mouse model of TCDD-Elicited Steatohepatitis. Toxicol Sci. 2016;154(2):381–91.
10. Rinella ME, Lazarus JV, Ratziu V, Francque SM, Sanyal AJ, Kanwal F, Romero D, Abdelmalek MF, Anstee QM, Arab JP, et al. A multisociety Delphi consensus statement on new fatty liver disease nomenclature. J Hepatol. 2023;79(6):1542–56.
11. Pierre S, Chevallier A, Teixeira-Clerc F, Ambolet-Camoit A, Bui LC, Bats AS, Fournet JC, Fernandez-Salguero P, Aggerbeck M, Lotersztajn S, et al. Aryl hydrocarbon receptor-dependent induction of liver fibrosis by dioxin. Toxicol Sci. 2014;137(1):114–24.
12. Geh D, Anstee QM, Reeves HL. NAFLD-Associated HCC: Progress and opportunities. J Hepatocell Carcinoma. 2021;8:223–39.
13. National Toxicology P. Carcinogenesis Bioassay of 2,3,7,8-Tetrachlorodibenzo-p-dioxin (CAS 1746-01-6) in swiss-Webster mice (dermal study). Natl Toxicol Program Tech Rep Ser. 1982;201:1–113.
14. Birnbaum LS, McDonald MM, Blair PC, Clark AM, Harris MW. Differential toxicity of 2,3,7,8-tetrachlorodibenzo-p-dioxin (TCDD) in C57BL/6J mice congenic at the Ah Locus. Fundam Appl Toxicol. 1990;15(1):186–200.
15. Vos JG, Moore JA, Zinkl JG. Toxicity of 2,3,7,8-tetrachlorodibenzo-p-dioxin (TCDD) in C57B1/6 mice. Toxicol Appl Pharmacol. 1974;29(2):229–41.
16. Cholico GN, Orlowska K, Fling RR, Sink WJ, Zacharewski NA, Fader KA, Nault R, Zacharewski T. Consequences of reprogramming acetyl-CoA metabolism by 2,3,7,8-tetrachlorodibenzo-p-dioxin in the mouse liver. Sci Rep. 2023;13(1):4138.
17. Tang J, Yan Z, Feng Q, Yu L, Wang H. The roles of neutrophils in the Pathogenesis of Liver diseases. Front Immunol. 2021;12:625472.
18. Su T, Yang Y, Lai S, Jeong J, Jung Y, McConnell M, Utsumi T, Iwakiri Y. Single-cell Transcriptomics reveals Zone-specific alterations of Liver Sinusoidal endothelial cells in cirrhosis. Cell Mol Gastroenterol Hepatol. 2021;11(4):1139–61.
19. Guilliams M, Bonnardel J, Haest B, Vanderborght B, Wagner C, Remmerie A, Bujko A, Martens L, Thone T, Browaeys R, et al. Spatial proteogenomics reveals distinct and evolutionarily conserved hepatic macrophage niches. Cell. 2022;185(2):379–96. e338.
20. Nault R, Fader KA, Bhattacharya S, Zacharewski TR. Single-nuclei RNA sequencing Assessment of the hepatic effects of 2,3,7,8-Tetrachlorodibenzo-p-dioxin. Cell Mol Gastroenterol Hepatol. 2021;11(1):147–59.
21. Stohs SJ. Oxidative stress induced by 2,3,7,8-tetrachlorodibenzo-p-dioxin (TCDD). Free Radic Biol Med. 1990;9(1):79–90.
22. Fader KA, Nault R, Kirby MP, Markous G, Matthews J, Zacharewski TR. Convergence of hepcidin deficiency, systemic iron overloading, heme accumulation, and REV-ERBalpha/beta activation in aryl hydrocarbon receptor-elicited hepatotoxicity. Toxicol Appl Pharmacol. 2017;321:1–17.
23. Nault R, Fader KA, Kirby MP, Ahmed S, Matthews J, Jones AD, Lunt SY, Zacharewski TR. Pyruvate kinase isoform switching and hepatic metabolic reprogramming by the Environmental Contaminant 2,3,7,8-Tetrachlorodibenzo-p-Dioxin. Toxicol Sci. 2016;149(2):358–71.
24. Cho TJ, Kim HJ, Cho J. Endothelin-converting enzyme-1 expression in acute and chronic liver injury in fibrogenesis. Anim Cells Syst (Seoul). 2019;23(3):170–5.
25. Zhao Y, Yu Y, Zhao W, You S, Feng M, Xie C, Chi X, Zhang Y, Wang X. As a downstream target of the AKT pathway, NPTX1 inhibits proliferation and promotes apoptosis in hepatocellular carcinoma. Biosci Rep 2019, 39(6).
26. Jiang M, Zeng Q, Dai S, Liang H, Dai F, Xie X, Lu K, Gao C. Comparative analysis of hepatocellular carcinoma and cirrhosis gene expression profiles. Mol Med Rep. 2017;15(1):380–6.
27. Xu Y, Zhu Y, Bawa FC, Hu S, Pan X, Yin L, Zhang Y. Hepatocyte-Specific Expression of Human Carboxylesterase 1 attenuates Diet-Induced Steatohepatitis and Hyperlipidemia in mice. Hepatol Commun. 2020;4(4):527–39.
28. Cholico GN, Fling RR, Zacharewski NA, Fader KA, Nault R, Zacharewski TR. Thioesterase induction by 2,3,7,8-tetrachlorodibenzo-p-dioxin results in a futile cycle that inhibits hepatic beta-oxidation. Sci Rep. 2021;11(1):15689.
29. Xie Y, Xie W. The role of sulfotransferases in Liver diseases. Drug Metab Dispos. 2020;48(9):742–9.
30. Van Loy T, De Jonghe S, Castermans K, Dheedene W, Stoop R, Verschuren L, Versele M, Chaltin P, Luttun A, Schols D. Stimulation of the atypical chemokine receptor 3 (ACKR3) by a small-molecule agonist attenuates fibrosis in a preclinical liver but not lung injury model. Cell Mol Life Sci. 2022;79(6):293.

31. Ma H, Liu X, Wang X, Wu T, Wang G, Lv G, Niu J. Transcriptome analysis of liver sinusoidal endothelial cells in patients with liver cirrhosis. In.: Research Square; 2023.
32. Xiong DD, Li JD, He RQ, Li MX, Pan YQ, He XL, Dang YW, Chen G. Highly expressed carbohydrate sulfotransferase 11 correlates with unfavorable prognosis and immune evasion of hepatocellular carcinoma. Cancer Med. 2023;12(4):4938–50.
33. Escudero-Esparza A, Bartoschek M, Gialeli C, Okroj M, Owen S, Jirstrom K, Orimo A, Jiang WG, Pietras K, Blom AM. Complement inhibitor CSMD1 acts as tumor suppressor in human breast cancer. Oncotarget. 2016;7(47):76920–33.
34. Wang X, Chen X, Liu Y, Huang S, Ding J, Wang B, Dong P, Sun Z, Chen L. CSMD1 suppresses cancer progression by inhibiting proliferation, epithelial-mesenchymal transition, chemotherapy-resistance and inducing immunosuppression in esophageal squamous cell carcinoma. Exp Cell Res. 2022;417(2):113220.
35. Vega-Benedetti AF, Saucedo CN, Zavattari P, Vanni R, Royo F, Llavero F, Zugaza JL, Parada LA. PLAGL1 gene function during hepatoma cells proliferation. Oncotarget. 2018;9(67):32775–94.
36. Raghuvanshi S, Reed V, Blaner WS, Harrison EH. Cellular localization of beta-carotene 15,15′ oxygenase-1 (BCO1) and beta-carotene 9′,10′ oxygenase-2 (BCO2) in rat liver and intestine. Arch Biochem Biophys. 2015;572:19–27.
37. Pavlakis E, Chiotaki R, Chalepakis G. The role of Fras1/Frem proteins in the structure and function of basement membrane. Int J Biochem Cell Biol. 2011;43(4):487–95.
38. Clugston RD. Carotenoids and fatty liver disease: current knowledge and research gaps. Biochim Biophys Acta Mol Cell Biol Lipids. 2020;1865(11):158597.
39. Lim JY, Liu C, Hu KQ, Smith DE, Wang XD. Ablation of carotenoid cleavage enzymes (BCO1 and BCO2) induced hepatic steatosis by altering the farnesoid X receptor/miR-34a/sirtuin 1 pathway. Arch Biochem Biophys. 2018;654:1–9.
40. Gianmoena K, Gasparoni N, Jashari A, Gabrys P, Grgas K, Ghallab A, Nordstrom K, Gasparoni G, Reinders J, Edlund K, et al. Epigenomic and transcriptional profiling identifies impaired glyoxylate detoxification in NAFLD as a risk factor for hyperoxaluria. Cell Rep. 2021;36(8):109526.
41. Sawitza I, Kordes C, Reister S, Haussinger D. The niche of stellate cells within rat liver. Hepatology. 2009;50(5):1617–24.
42. Tecalco-Cruz AC, Sosa-Garrocho M, Vazquez-Victorio G, Ortiz-Garcia L, Dominguez-Huttinger E, Macias-Silva M. Transforming growth factor-beta/SMAD target gene SKIL is negatively regulated by the transcriptional cofactor complex SNON-SMAD4. J Biol Chem. 2012;287(32):26764–76.
43. Rava M, D'Andrea A, Doni M, Kress TR, Ostuni R, Bianchi V, Morelli MJ, Collino A, Ghisletti S, Nicoli P, et al. Mutual epithelium-macrophage dependency in liver carcinogenesis mediated by ST18. Hepatology. 2017;65(5):1708–19.
44. Lyons YA, Wu SY, Overwijk WW, Baggerly KA, Sood AK. Immune cell profiling in cancer: molecular approaches to cell-specific identification. NPJ Precis Oncol. 2017;1(1):26.
45. Park DD, Chen J, Kudelka MR, Jia N, Haller CA, Kosaraju R, Premji AM, Galizzi M, Nairn AV, Moremen KW, et al. Resident and elicited murine macrophages differ in expression of their glycomes and glycan-binding proteins. Cell Chem Biol. 2021;28(4):567–e582564.
46. Niederkorn M, Agarwal P, Starczynowski DT. TIFA and TIFAB: FHA-domain proteins involved in inflammation, hematopoiesis, and disease. Exp Hematol. 2020;90:18–29.
47. Boverhof DR, Burgoon LD, Tashiro C, Chittim B, Harkema JR, Jump DB, Zacharewski TR. Temporal and dose-dependent hepatic gene expression patterns in mice provide new insights into TCDD-Mediated hepatotoxicity. Toxicol Sci. 2005;85(2):1048–63.
48. Ito M, Jiang C, Krumm K, Zhang X, Pecha J, Zhao J, Guo Y, Roeder RG, Xiao H. TIP30 deficiency increases susceptibility to tumorigenesis. Cancer Res. 2003;63(24):8763–7.
49. Farber MJ, Rizaldy R, Hildebrand JD. Shroom2 regulates contractility to control endothelial morphogenesis. Mol Biol Cell. 2011;22(6):795–805.
50. O'Brien MH, Pitot HC, Chung SH, Lambert PF, Drinkwater NR, Bilger A. Estrogen receptor-alpha suppresses liver carcinogenesis and establishes sex-specific gene expression. Cancers (Basel) 2021, 13(10).
51. Cholico GN, Fling RR, Sink WJ, Nault R, Zacharewski T. Inhibition of the urea cycle by the environmental contaminant 2,3,7,8-tetrachlorodibenzo-p-dioxin increases serum ammonia levels in mice. J Biol Chem 2023:105500.
52. Zheng R, Zhu HL, Hu BR, Ruan XJ, Cai HJ. Identification of APEX2 as an oncogene in liver cancer. World J Clin Cases. 2020;8(14):2917–29.
53. Boucheron N, Ellmeier W. The role of Tec family kinases in the regulation of T-helper-cell differentiation. Int Rev Immunol. 2012;31(2):133–54.
54. Yang X, Guo J, Li W, Li C, Zhu X, Liu Y, Wu X. PPM1H is down-regulated by ATF6 and dephosphorylates p-RPS6KB1 to inhibit progression of hepatocellular carcinoma. Mol Ther Nucleic Acids. 2023;33:164–79.
55. Naeim F. Principles of Immunophenotyping. In: *Hematopathology.* Edited by Naeim F, Rao PN, Grody WW. Oxford: Academic Press; 2008: 27–55.
56. Yang H, Arif M, Yuan M, Li X, Shong K, Turkez H, Nielsen J, Uhlen M, Boren J, Zhang C, et al. A network-based approach reveals the dysregulated transcriptional regulation in non-alcoholic fatty liver disease. iScience. 2021;24(11):103222.
57. Chen CC, Xie XM, Zhao XK, Zuo S, Li HY. Kruppel-like factor 13 promotes HCC Progression by Transcriptional Regulation of HMGCS1-mediated cholesterol synthesis. J Clin Transl Hepatol. 2022;10(6):1125–37.
58. Wang PR, Xu M, Toffanin S, Li Y, Llovet JM, Russell DW. Induction of hepatocellular carcinoma by in vivo gene targeting. Proc Natl Acad Sci U S A. 2012;109(28):11264–9.
59. Wang Q, Tang Q, Zhao L, Zhang Q, Wu Y, Hu H, Liu L, Liu X, Zhu Y, Guo A, et al. Time serial transcriptome reveals Cyp2c29 as a key gene in hepatocellular carcinoma development. Cancer Biol Med. 2020;17(2):401–17.
60. Lin P, He RQ, Dang YW, Wen DY, Ma J, He Y, Chen G, Yang H. An autophagy-related gene expression signature for survival prediction in multiple cohorts of hepatocellular carcinoma patients. Oncotarget. 2018;9(25):17368–95.
61. Nault R, Cholico GN, Zacharewski T. Analysis of cell-cell communication by single-nuclei RNA sequencing identifies AHR-Mediated induction of NRG-ERBB signaling. Receptors. 2023;2(2):148–59.
62. Couper MR, Brown RM, Gupte G, Perera M, Kelgeri C. Liver Disease in GLIS3 mutations: transplant considerations and bile Duct Paucity on Explant Histology. J Pediatr Gastroenterol Nutr. 2023;77(1):110–4.
63. Celius T, Roblin S, Harper PA, Matthews J, Boutros PC, Pohjanvirta R, Okey AB. Aryl hydrocarbon receptor-dependent induction of flavin-containing monooxygenase mRNAs in mouse liver. Drug Metab Dispos. 2008;36(12):2499–505.
64. Massey W, Osborn LJ, Banerjee R, Horak A, Fung KK, Orabi D, Chan ER, Sangwan N, Wang Z, Brown JM. Flavin-Containing monooxygenase 3 (FMO3) is critical for Dioxin-Induced reorganization of the gut microbiome and host insulin sensitivity. Metabolites 2022, 12(4).
65. Zhang T, Zhang N, Xing J, Zhang S, Chen Y, Xu D, Gu J. UDP-glucuronate metabolism controls RIPK1-driven liver damage in nonalcoholic steatohepatitis. Nat Commun. 2023;14(1):2715.
66. Soltis AR, Kennedy NJ, Xin X, Zhou F, Ficarro SB, Yap YS, Matthews BJ, Lauffenburger DA, White FM, Marto JA, et al. Hepatic dysfunction caused by consumption of a high-Fat Diet. Cell Rep. 2017;21(11):3317–28.
67. Yeager RL, Reisman SA, Aleksunes LM, Klaassen CD. Introducing the TCDD-inducible AhR-Nrf2 gene battery. Toxicol Sci. 2009;111(2):238–46.
68. Wu M, Jiang L. Hydroxysteroid 17-Beta dehydrogenase 6 is a prognostic biomarker and correlates with Immune infiltrates in Hepatocellular Carcinoma. Dig Dis Sci. 2022;67(1):146–58.
69. Hazlehurst JM, Oprescu AI, Nikolaou N, Di Guida R, Grinbergs AE, Davies NP, Flintham RB, Armstrong MJ, Taylor AE, Hughes BA, et al. Dual-5alpha-Reductase inhibition promotes hepatic lipid Accumulation in Man. J Clin Endocrinol Metab. 2016;101(1):103–13.
70. Xu C, Li H, Tang CK. Sterol carrier protein 2 in lipid metabolism and non-alcoholic fatty liver disease: pathophysiology, molecular biology, and potential clinical implications. Metabolism. 2022;131:155180.
71. Vilarinho S, Sari S, Mazzacuva F, Bilguvar K, Esendagli-Yilmaz G, Jain D, Akyol G, Dalgic B, Gunel M, Clayton PT, et al. ACOX2 deficiency: a disorder of bile acid synthesis with transaminase elevation, liver fibrosis, ataxia, and cognitive impairment. Proc Natl Acad Sci U S A. 2016;113(40):11289–93.
72. Lee JH, Wada T, Febbraio M, He J, Matsubara T, Lee MJ, Gonzalez FJ, Xie W. A novel role for the Dioxin receptor in fatty acid metabolism and Hepatic Steatosis. Gastroenterology. 2010;139(2):653–63.
73. Nault R, Fader KA, Lydic TA, Zacharewski TR. Lipidomic Evaluation of Aryl Hydrocarbon receptor-mediated hepatic steatosis in male and female mice elicited by 2,3,7,8-Tetrachlorodibenzo-p-dioxin. Chem Res Toxicol. 2017;30(4):1060–75.
74. Unkila M, Pohjanvirta R, MacDonald E, Tuomisto JT, Tuomisto J. Dose response and time course of alterations in tryptophan metabolism by 2,3,7,8-tetrachlorodibenzo-p-dioxin (TCDD) in the most TCDD-susceptible and the most TCDD-resistant rat strain: relationship with TCDD lethality. Toxicol Appl Pharmacol. 1994;128(2):280–92.

75. Li J, Li Y, Sha R, Zheng L, Xu L, Xie HQ, Zhao B. Effects of perinatal TCDD exposure on colonic microbiota and metabolism in offspring and mother mice. Sci Total Environ. 2022;832:154762.
76. Unkila M, Ruotsalainen M, Pohjanvirta R, Viluksela M, MacDonald E, Tuomisto JT, Rozman K, Tuomisto J. Effect of 2,3,7,8-tetrachlorodibenzo-p-dioxin (TCDD) on tryptophan and glucose homeostasis in the most TCDD-susceptible and the most TCDD-resistant species, guinea pigs and hamsters. Arch Toxicol. 1995;69(10):677–83.
77. Unkila M, Pohjanvirta R, Tuomisto J. Body weight loss and changes in tryptophan homeostasis by chlorinated dibenzo-p-dioxin congeners in the most TCDD-susceptible and the most TCDD-resistant rat strain. Arch Toxicol. 1998;72(12):769–76.
78. Li L, Wang T, Li S, Chen Z, Wu J, Cao W, Wo Q, Qin X, Xu J. TDO2 promotes the EMT of Hepatocellular Carcinoma through Kyn-AhR pathway. Front Oncol. 2020;10:562823.
79. Rehati A, Abuduaini B, Liang Z, Chen D, He F. Identification of heat shock protein family a member 5 (HSPA5) targets involved in nonalcoholic fatty liver disease. Genes Immun. 2023;24(3):124–9.
80. Duan Z, Zhao J, Fan X, Tang C, Liang L, Nie X, Liu J, Wu Q, Xu G. The PERK-eIF2alpha signaling pathway is involved in TCDD-induced ER stress in PC12 cells. Neurotoxicology. 2014;44:149–59.
81. Chen Y, Yang Y, Miller ML, Shen D, Shertzer HG, Stringer KF, Wang B, Schneider SN, Nebert DW, Dalton TP. Hepatocyte-specific gclc deletion leads to rapid onset of steatosis with mitochondrial injury and liver failure. Hepatology. 2007;45(5):1118–28.
82. Kamm DR, McCommis KS. Hepatic stellate cells in physiology and pathology. J Physiol. 2022;600(8):1825–37.
83. O'Byrne SM, Blaner WS. Retinol and retinyl esters: biochemistry and physiology. J Lipid Res. 2013;54(7):1731–43.
84. Sheikh E, Tran T, Vranic S, Levy A, Bonfil RD. Role and significance of c-KIT receptor tyrosine kinase in cancer: a review. Bosn J Basic Med Sci. 2022;22(5):683–98.
85. Fling RR, Doskey CM, Fader KA, Nault R, Zacharewski TR. 2,3,7,8-Tetrachlorodibenzo-p-dioxin (TCDD) dysregulates hepatic one carbon metabolism during the progression of steatosis to steatohepatitis with fibrosis in mice. Sci Rep. 2020;10(1):14831.
86. Ghosh AK, Vaughan DE. PAI-1 in tissue fibrosis. J Cell Physiol. 2012;227(2):493–507.
87. Percie du Sert N, Hurst V, Ahluwalia A, Alam S, Avey MT, Baker M, Browne WJ, Clark A, Cuthill IC, Dirnagl U, et al. The ARRIVE guidelines 2.0: updated guidelines for reporting animal research. BMC Vet Res. 2020;16(1):242.
88. Wolock SL, Lopez R, Klein AM. Scrublet: computational identification of cell doublets in single-cell Transcriptomic Data. Cell Syst. 2019;8(4):281–e291289.
89. Wolf FA, Angerer P, Theis FJ. SCANPY: large-scale single-cell gene expression data analysis. Genome Biol. 2018;19(1):15.
90. Squair JW, Gautier M, Kathe C, Anderson MA, James ND, Hutson TH, Hudelle R, Qaiser T, Matson KJE, Barraud Q, et al. Confronting false discoveries in single-cell differential expression. Nat Commun. 2021;12(1):5692.
91. McCarthy DJ, Campbell KR, Lun ATL, Wills QF. Scater: pre-processing, quality control, normalization and visualization of single-cell RNA-seq data in R. Bioinformatics. 2017;33(8):1179–86.
92. Love MI, Huber W, Anders S. Moderated estimation of Fold change and dispersion for RNA-seq data with DESeq2. Genome Biol. 2014;15(12):550.
93. Fang Z, Liu X, Peltz G. GSEApy: a comprehensive package for performing gene set enrichment analysis in Python. Bioinformatics. 2023;39(1):btac757.
94. Cholico GN, Nault R, Zacharewski TR. Genome-wide ChIPseq analysis of AhR, COUP-TF, and HNF4 Enrichment in TCDD-Treated mouse liver. Int J Mol Sci. 2022;23(3):1558.
95. Liming L, Jason H, Valerie B, Eun Woo S, Yuguang B, Wei W, Jianli Q, Gaixin J, Arthur L. Steven Xijin G: GSKB: a gene set database for pathway analysis in mouse. bioRxiv 2016:082511.

Publisher's note